

Tutorial

Invasive and Non-Invasive Observation of Occluded Fast Transient Events: Computational Tools

Soon Hock Ng ^{1,†} , Vijayakumar Anand ^{1,*,†} , Tomas Katkus ¹ and Saulius Juodkazis ^{1,2} 

¹ Optical Sciences Centre and ARC Training Centre in Surface Engineering for Advanced Materials (SEAM), School of Science, Swinburne University of Technology, Hawthorn, VIC 3122, Australia; soonhockng@swin.edu.au (S.H.N.); tkatkus@swin.edu.au (T.K.); sjuodkazis@swin.edu.au (S.J.)

² Tokyo Tech World Research Hub Initiative (WRHI), School of Materials and Chemical Technology, Tokyo Institute of Technology, 2-12-1, Ookayama, Meguro-ku, Tokyo 152-8550, Japan

* Correspondence: vanand@swin.edu.au

† The authors contributed equally to this work.

Abstract: Industrial processes involving thermal plasma such as cutting, welding, laser machining with ultra-short laser pulses (nonequilibrium conditions), high temperature melting using electrical discharge or ion-beams, etc., generate non-repeatable fast transient events which can reveal valuable information about the processes. In such industrial environments containing high temperature and radiation, it is often difficult to install conventional lens-based imaging windows and components to observe such events. In this study, we compare imaging requirements and performances with invasive and non-invasive modes when a fast transient event is occluded by a metal window consisting of numerous holes punched through it. Simulation studies were carried out for metal windows with different types of patterns, reconstructed for both invasive and non-invasive modes and compared. Sparks were generated by rapid electrical discharge behind a metal window consisting of thousands of punched through-holes and the time sequence was recorded using a high-speed camera. The time sequence was reconstructed with and without the spatio-spectral point spread functions and compared. Commented MATLAB codes are provided for both invasive and non-invasive modes of reconstruction.

Keywords: fast transient events; high-speed imaging; computational optics; holography; diffraction; phase-retrieval algorithm; invasive imaging; non-invasive imaging



Citation: Ng, S.H.; Anand, V.; Katkus, T.; Juodkazis, S. Invasive and Non-Invasive Observation of Occluded Fast Transient Events: Computational Tools. *Photonics* **2021**, *8*, 253. <https://doi.org/10.3390/photonics8070253>

Received: 31 May 2021

Accepted: 29 June 2021

Published: 1 July 2021

Publisher's Note: MDPI stays neutral with regard to jurisdictional claims in published maps and institutional affiliations.



Copyright: © 2021 by the authors. Licensee MDPI, Basel, Switzerland. This article is an open access article distributed under the terms and conditions of the Creative Commons Attribution (CC BY) license (<https://creativecommons.org/licenses/by/4.0/>).

1. Introduction

Imaging through occlusion such as mist, fog, or a scattering medium is a challenging task [1–3]. There are many techniques developed which allows reconstruction of the object information from the deformed images [3–6]. Techniques which utilize the information of the imaging configuration such as the point spread function (PSF), scattering matrix, and distances are categorized as invasive since additional information related to the scattering media is needed [4]. The techniques which do not require any of the information as described above are classified as non-invasive [5,6].

The two modes: invasive and non-invasive have their own advantages and disadvantages. The requirement of additional information about the imaging components and configuration in invasive mode is the disadvantage but the method can reconstruct up to 5D information in space, spectrum, and time [7,8]. In non-invasive approaches, the capability is often limited to 2D [6]. In the recent years, there has been numerous research works on non-invasive approaches and the method has been successfully extended to obtain an additional dimension—depth [9–11]. Another major difference between invasive and non-invasive approaches is that with invasive methods, it is possible to reconstruct the object information as close as possible to reality, with higher signal to noise ratio (SNR), optimal resolution and field of view. In the non-invasive approaches, the demonstration is

often carried out with much smaller objects and the quality of reconstructions are much lower than direct and invasive approaches. Furthermore, the non-invasive approach relies on an initial guess (random matrix) which controls the degree of convergence, necessitating several initial guess cases in [6], that were tried until an optimal reconstruction was obtained.

In this tutorial, a comprehensive comparison of different types of correlation based invasive reconstruction methods and non-invasive type reconstruction using phase-retrieval algorithm is studied. The manuscript consists of five sections. In the next section, the methodology of the study is described. The simulative studies are presented in third section. The computational reconstruction with MATLAB code is described in the fourth section. In the fifth section, the experimental results are presented and discussed. The conclusion and summary are presented in the final section. Supplementary files consisting of original MATLAB code with comments are provided for a freshman in this area of research.

2. Methodology

The optical configuration of light collection from an isolated fast transient industrial process through an occlusion (metal window with holes) by a ultra-high-speed camera is shown in Figure 1. Many industrial processes produce intense temperature, light intensity, and pressure so are generally isolated from their surroundings. This makes it difficult to image or monitor using conventional lens-based imaging systems. A metal occlusion consisting of few holes is better than a glass window as it can substantially cut down the light intensity. Additionally, an electrical bias of such “metallic-optics” can be used to mitigate material (re)deposition for a close placement of them near high-temperature event. Furthermore, if the holes have sizes of the order of the wavelength of interest then the light will undergo diffraction and generate intensities within recordable range of values. Let us consider that the fast transient event generates light that is spatially as well as temporally incoherent (Figure 1).

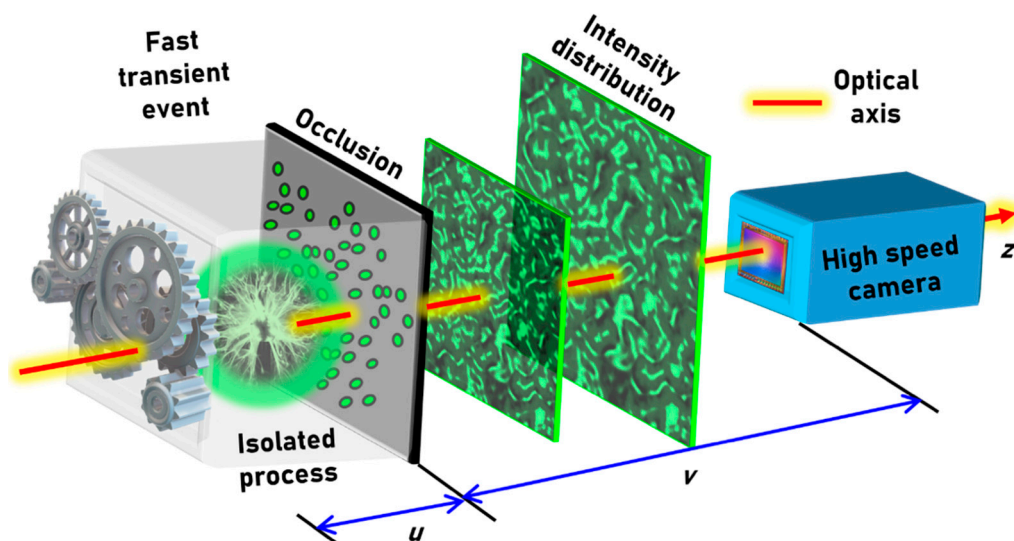


Figure 1. Optical configuration of light collection from an isolated fast transient industrial process through an occlusion (metal window with punched holes) by a high-speed camera.

As it is seen in Figure 1, what is recorded by the high-speed camera is not the image of the object or the event but a scattered intensity distribution. Therefore, the recorded intensity distribution needs to be processed to reconstruct the event as close as possible to reality. This reconstruction can be achieved using two modes: invasive and non-invasive. In the invasive approach, as the name suggests it is necessary to carry out some measurements in the region invasively where the event occurs to extract additional information about the

system. This invasion can be either in the form of recording the image of the occlusion and generating the transmission matrix or mounting a point object such as a pinhole at different axial locations and recording the PSF library. The above invasion is possible in some cases and may be safe where the space beyond the occlusion is accessible or the occlusion itself is detachable. In such cases, a PSF library can be recorded for different wavelengths or the occlusion can be imaged. By processing the PSF library with the recorded scattered intensity distribution, the event can be completely reconstructed in depth and wavelength up to five dimensions. However, in many industrial processors, the above is not possible where the occlusion is welded on to the system and the space beyond the occlusion is not accessible. Besides, this invasive procedure is especially not safe in biomedical applications where the surface of an organ or tissue is occluded by the skin. In such cases, the only information that is available is the scattered intensity distribution and the reconstruction mechanisms which use only this scattered intensity distribution are called as non-invasive imaging methods. Phase-retrieval based image reconstruction techniques that can reconstruct the event or the image of the object just by processing only the scattered intensity distribution without any other information of the system were developed. However, is the phase retrieval-based reconstruction universal? i.e., does this approach work in all types of occlusions? In the next sections, the mathematical formulations are presented and simulative studies on different types of occlusions are investigated.

2.1. Invasive

Let $I_o(\lambda)$ be the intensity of a point object emitting light with a wavelength λ , located in the (x_o, y_o) plane at a distance of u from the occluding object. The complex amplitude at the occlusion is given by

$$\psi_1 = C_1 \sqrt{I_o(\lambda)} L(\bar{o}/u) Q(1/u), \tag{1}$$

where $\bar{r}_o = (x_o, y_o)$, $L(\bar{o}/u) = \exp[j2\pi(o_x x + o_y y)/(\lambda u)]$ and $Q(1/u) = \exp[j\pi(x^2 + y^2)/(\lambda u)]$ are the linear and quadratic phase factors respectively, C_1 is a complex constant and $o_x x$ and $o_y y$ are the projections along the x and y directions. Considering the occlusion as a metal consisting of many holes of the order of wavelength, the following design can be made. The occlusion at a plane m consisting of N micro-holes that are randomly located can be expressed as

$$Mask = \sum_{i=1}^N \delta(\bar{r} - \bar{r}_{i,m}) \otimes circ(R) \tag{2}$$

where $\delta(\bar{r} - \bar{r}_{i,m})$ is a Delta function, R is the radius of the pinhole and ' \otimes ' is a two dimensional (2D) convolutional operator, $\bar{r}_m = (x_m, y_m)$, $\bar{r}_i = (x_i, y_i)$ and $x_i, y_i \in \{C_2 \cdot (U[0, 1])\}$, U is a uniform random variable distributed on $[0, C_2]$ and $circ(R)$ is the circle function. The above convolution operation creates holes in the locations of the Delta functions. The complex amplitude after the mask is given as

$$\psi_2 = C_1 \sqrt{I_o(\lambda)} L(\bar{o}/u) Q(1/u) Mask \tag{3}$$

The sensor located at a distance of v from the occlusion records an intensity distribution given by

$$I_{PSF}(\bar{r}_s; \bar{r}_o, u, \lambda) = \left| C_1 \sqrt{I_o(\lambda)} L\left(\frac{\bar{o}}{u}\right) Q\left(\frac{1}{u}\right) Mask \otimes Q\left(\frac{1}{v}\right) \right|^2, \tag{4}$$

where \bar{r}_s is the location vector in the sensor plane. The above equation can be modified as

$$I_{PSF}(\bar{r}_s; \bar{r}_o, u, \lambda) = I_{PSF}\left(\bar{r}_s - \frac{v}{u} \bar{r}_o; 0, u, \lambda\right) \tag{5}$$

which indicates that a point in the object plane located not along the optical axis will generate the same intensity pattern but shifted in the sensor plane by $\frac{v}{u}\bar{r}_o$. So, the location vector is modified by including this shift. A 2D object consisting of multiple points can be represented as

$$o(\bar{r}_o) = \sum_i a_i \delta(r - r_i), \tag{6}$$

where a_i is the intensity at the object plane (at the point i). The object intensity pattern at the sensor plane is given as

$$O(\bar{r}_s, u, \lambda) = \sum_i a_i I_{\text{PSF}}\left(\bar{r}_s - \frac{v}{u}\bar{r}_{o,i}; 0, u, \lambda\right) \tag{7}$$

The image of the object is reconstructed by a cross-correlation between O and I_{PSF}

$$I_R(\bar{r}_R) = \iint \sum_i a_i I_{\text{PSF}}\left(\bar{r}_s - \frac{v}{u}\bar{r}_{o,i}; u, \lambda\right) I_{\text{PSF}}^*(\bar{r}_s - \bar{r}_R; u, \lambda), = \left[\iint \sum_i a_i \Lambda\left(\bar{r}_R - \frac{v}{u}\bar{r}_{o,i}\right) \right] + K \approx o\left(\frac{\bar{r}_s}{M}\right) + K, \tag{8}$$

where M is the magnification of the system given by v/u and Λ is a Delta-like function which samples the object and K is a function indicating background noise arising due to cross-correlating two positive functions. If the conditions of either the object or the point object in u or λ are different from one another, then the width of Λ increases with the minimal width corresponding to $\sim 2.44\lambda/\text{NA}$ when there is a perfect match in wavelength and distance. The above correlation can be accomplished through different filters such as matched filter [12], phase-only filter [13], non-linear filter (NLR) [14], Weiner filter (WF) [15] and other algorithms such as Lucy–Richardson algorithm (LRA) [16,17], maximum likelihood algorithm (MLA) [18], regularized filter algorithm (RFA) [19]. The previous studies [20] have proven that the NLR has better performance than different filters and iterative methods due to the high level of adaptability and versatility [20].

2.2. Non-Invasive

In non-invasive approach, the reconstruction is not by a cross-correlation with the PSF but by a phase-retrieval algorithm which uses the magnitude of the autocorrelation of the object intensity distribution given as $I_A = O * O$, where ‘*’ is a 2D correlation operator. Rewriting the above expression by expanding the object intensity distribution O , we get $I_A = (o \otimes I_{\text{PSF}}) * (o \otimes I_{\text{PSF}})$. The terms can be rearranged by convolution theorem such that $I_A = (o * o) \otimes (I_{\text{PSF}} * I_{\text{PSF}})$ [21]. The autocorrelation of I_{PSF} gives rise to a Delta-like function Λ with a background given by K and so $I_A = (o * o) \otimes (\Lambda + K)$. The function of K is given by the nature of the occlusion as described in [22]. So, the above expression can be written as $I_A = (o * o + K_1)$. For simplicity, the occlusion is considered as highly scattering and so K_1 is nearly constant which can be suppressed by subtraction of the average minimum value. The autocorrelation of the object intensity distribution can be expressed in terms of Fourier transforms as $I_A = \mathfrak{F}^{-1}\left\{|\mathfrak{F}\{O\}|^2\right\}$ [23]. A Fourier transform operation followed by a square root on I_A will result in $|\mathfrak{F}\{O\}|$. As the magnitude of Fourier transform of the object information is available, the object information can be obtained using Fienup type phase retrieval algorithm [24].

The block diagram for the phase-retrieval algorithm is shown in Figure 2. In the first step, the autocorrelation of the object intensity distribution is calculated, followed by a Fourier transform and square root operation yielding the magnitude of the Fourier transform of the object. There are two planes of interest with complex amplitudes $A_1(x, y)$ and $\sqrt{|\mathfrak{F}\{I_A(k_x, k_y)\}}|\exp[j\Phi(k_x, k_y)]$ as shown in Figure 2. The size of $A_1(x, y)$ is predicted as approximately half of the extend of I_A as the autocorrelation of the intensity is equivalent to the autocorrelation of the object if the autocorrelation of the PSF generates a Delta-like function. The algorithm begins with an initial guess object function $A_1(x, y)$ with a size about half of the width of I_A and a value of zero for all other pixels of the matrix. This

matrix is Fourier transformed and the resulting complex amplitude's real part is replaced by $\sqrt{|\Im\{I_A(k_x, k_y)\}|}$ while the phase $\Phi(k_x, k_y)$ was carried on. The resulting matrix is inverse Fourier transformed and the constraints of non-negativity and real are applied and this process is iterated until the matrix $A_1(x, y)$ converges and reaches non-changing values. Thus, the object function is reconstructed. Previous studies have indicated that convergence of the algorithm is highly dependent upon the initial guess matrices and so it was repeated many numbers of times with different initial guess matrices mostly with a random profile [6].

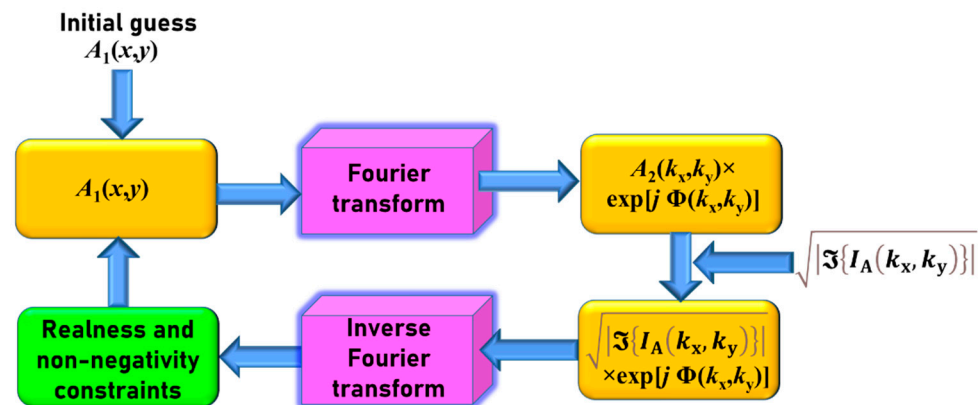


Figure 2. Block diagram of the phase-retrieval algorithm.

3. Simulative Studies

In this section, the invasive and non-invasive approaches were studied for different types of occlusion as shown in Figure 3a–d and for an object consisting of two circular objects as shown in Figure 3e. The previous studies have shown that the non-invasive approaches work well only for simpler objects with a smaller field of view [6]. The main difference between Figure 3a–d is that the first three are periodic structures while the final one is chaotic [7]. Even though the inversion images of Figure 3a,b are typically used, the current images were used for decreasing the light throughput. The simulation studies were carried out and the PSFs are shown in Figure 4. As is seen, the periodic structures generate PSFs that have periodic intensity patterns. Consequently, the autocorrelation of the periodic patterns give rise to multiple peaks other than a single peak as described in Section 2. For this reason, the generated function cannot be considered as a Delta-like function for the periodic cases. The object intensity distributions for different cases are simulated by convolving the respective PSFs with the object function shown in Figure 3e. As expected, the object intensity distribution appears periodic except for the case with randomly punched holes. The phase retrieval method has been applied to reconstruct the object information without the PSF and the results for different types of occlusion are shown in Figure 4. As expected, the reconstruction for periodic intensity cases have lower quality than the case with randomly punched holes. The invasive approach was implemented with NLR given as $I_R = \left| \mathcal{F}^{-1} \left\{ \left| \tilde{I}_{PSF} \right|^\alpha \exp \left[i \arg \left(\tilde{I}_{PSF} \right) \right] \left| \tilde{O} \right|^\beta \exp \left[-i \arg \left(\tilde{O} \right) \right] \right\} \right|$ and the parameters α and β are tuned between -1 and 1 until a minimum entropy given as $S(p, q) = - \sum \sum \phi(m, n) \log[\phi(m, n)]$, is obtained where $\phi(m, n) = |C(m, n)| / \sum \sum_{M, N} |C(m, n)|$, (m, n) are the indexes of the correlation matrix, and $C(m, n)$ is the correlation distribution. The reconstruction results are better for the case with random intensity distribution than other cases of occlusion with periodic mesh patterns. The results shown in the rows 4 and 5 (from top) of Figure 4 are magnified versions of the reconstructed images with the central part filling up the window. Every reconstructed pixel information of the reconstructed image is approximately twice the size of the diffraction limited spot as the object function o is sampled by the autocorrelation function of the imaging system. The image reconstruction

by NLR can be given as $I_O = O * I_{PSF} = (o \otimes I_{PSF}) * I_{PSF}$. Rearranging the terms of the equation we get $o \otimes (I_{PSF} * I_{PSF}) = o \otimes \Lambda$, where Λ is twice the diffraction limited spot size for matched filter [13] and can be equal to the size of the diffraction limited spot size at the optimal case of the NLR [14].

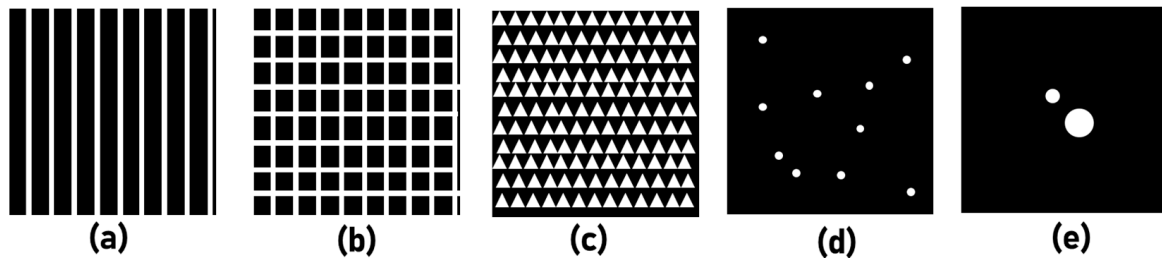


Figure 3. Intensity images of different types of occlusion (a) 1-D mesh, (b) 2D mesh, (c) triangular mesh and (d) block with randomly arranged holes. (e) Image of the object. The white regions indicate the opening, and the dark regions indicate the metal block.

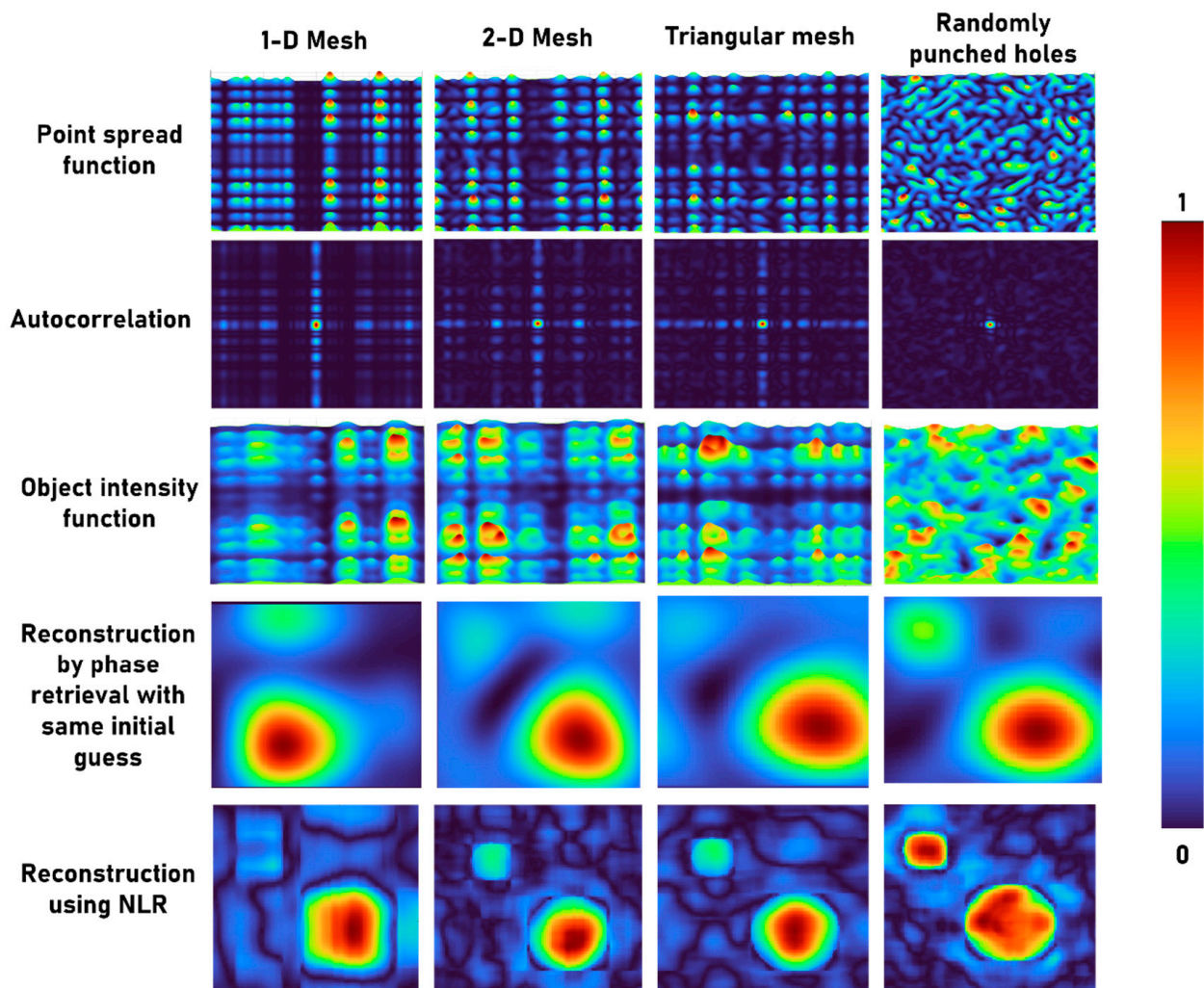


Figure 4. Simulated PSF, autocorrelation of PSF, object intensity function, reconstruction using phase retrieval and NLR Figure 1. D mesh, 2-D mesh, triangular mesh and randomly arranged holes in a metal plate. All the images are normalized to a range of values between 0 and 1.

4. Software

The computational reconstruction has been carried out using the software MATLAB. The step-by-step approach is provided using pseudo code for invasive and non-invasive cases in Tables 1 and 2 respectively. In invasive mode, there are two inputs namely the object intensity pattern and the PSF and in non-invasive mode, there is only a single input which is the object intensity distribution. In invasive mode, the reconstruction is direct where the matrices of object intensity pattern and PSF are cross correlated by NLR filter. By setting different values to α and β , different filters such as matched filter, phase-only filter and Weiner or inverse filter cases can be obtained. Other iterative reconstruction methods such as LRA and MLA and noise removal method RFA are available as one line syntax in MATLAB software. The pre-processing of the recorded intensity distributions is similar in both cases.

Table 1. Pseudocode for the reconstruction of the image for invasive mode of imaging through occlusion.

Task. No	Task	Steps
1	Defining computational space	Step-I Define the length and breadth of the computational space in pixels (N_1, N_2). Step-II Define origin (0, 0), x and y coordinates: $x = (1 \text{ to } N_1), y = (1 \text{ to } N_2)$. Step-III Create meshgrid: $(X, Y) = \text{meshgrid}(x, y)$.
2	Load experimentally recorded object intensity pattern and PSF and carry out low pass filtering	Step-I Read image files of object intensity pattern and PSF and convert them into double precision arrays and choose one of the channels of RGB. Step-II Define radial coordinate using the coordinates of the meshgrid $R = \sqrt{(X - N/2)^2 + (Y - N/2)^2}$. Calculate Fourier transform of the two processed matrices $\mathfrak{S}\{O'\}$ and $\mathfrak{S}\{I_{\text{PSF}}'\}$ and select the radial range of spatial frequencies (For $R > r$, $\mathfrak{S}\{O'\} = 0$ and $\mathfrak{S}\{I_{\text{PSF}}'\} = 0$) calculate the inverse Fourier transform, where the prime symbol indicates processed matrices and r is the spatial frequency range. The absolute value of the resulting matrices namely O'' and I_{PSF}'' can be used for further processing.
3	Reconstruction	Normalise O'' and I_{PSF}'' . Step-I Calculate Fourier transform of O'' and I_{PSF}'' $\mathfrak{S}\{O''\}$ and $\mathfrak{S}\{I_{\text{PSF}}''\}$. Step-II Multiply $\mathfrak{S}\{O''\}$ with $\mathfrak{S}\{I_{\text{PSF}}''\}$ for different values of α and β ranging from -1 to 1 in steps of 0.1 and calculate inverse Fourier transform. Calculate entropy and find the optimal reconstruction. $\alpha = 1$, and $\beta = 1$, Matched filter. $\alpha = 0$, and $\beta = 1$, Phase-only filter. $\alpha = -1$, and $\beta = 1$, Weiner or inverse filter. Step-III Apply median filter to the optimal reconstruction. Step-IV Display the result.

Table 2. Pseudocode for the reconstruction of the image for non-invasive mode of imaging through occlusion.

Task. No	Task	Steps
1	Defining computational space	Step-I Define the length and breadth of the computational space in pixels (N_1, N_2). Step-II Define origin (0, 0), x and y coordinates: $x = (1 \text{ to } N_1), y = (1 \text{ to } N_2)$. Step-III Create meshgrid: $(X, Y) = \text{meshgrid}(x, y)$.
2	Load experimentally recorded object intensity pattern, carry out low pass filtering and autocorrelation and determine parameters	Step-I Read image files of object intensity pattern, convert it into double precision arrays and choose one of the channels of RGB. Step-II Define radial coordinate using the coordinates of the meshgrid $R = \sqrt{(X - N/2)^2 + (Y - N/2)^2}$. Calculate Fourier transform of the processed matrix $\mathfrak{S}\{O'\}$ and select the radial range of spatial frequencies (For $R > r, \mathfrak{S}\{O'\} = 0$) calculate the inverse Fourier transform, where the prime symbol indicates processed matrices and r is the spatial frequency range. The absolute value of the resulting matrix namely O'' is extracted, the minimum value was subtracted and normalized again. The magnitude of Fourier transform of the object is calculated as $\sqrt{ \mathfrak{S}[\mathfrak{S}^{-1}\{ \mathfrak{S}\{O\} ^2\}] }$ which is used in the phase retrieval algorithm. Step-III Set the size of the object and generate the initial guess object function from the extension of the autocorrelation function and low pass filter.
3	Phase retrieval algorithm (Figure 2)	Start for loop Step-I Calculate Fourier transform of the initial guess object matrix $A_1(x, y)$ which produces $A_2(x, y)\exp[j\Phi(k_x, k_y)]$. Step-II Replace $A_2(x, y)$ by $\sqrt{ \mathfrak{S}[\mathfrak{S}^{-1}\{ \mathfrak{S}\{O\} ^2\}] }$ and calculate inverse Fourier transform. Step-III Apply constraints—real and object size. End for loop

5. Experiments

The schematic of the experimental set up is exactly same as the optical configuration shown in Figure 1. A spark is generated behind an occlusion and the scattered intensity pattern was recorded using an ultra-high-speed camera. The spark generation circuit is shown in Figure 5a and the photograph of the experimental set up is shown in Figure 5b. The occlusion for the experiment was fabricated on a 4-inch chromium coated glass plate with a thin layer of resist. A design consisting of 12,000 holes grouped into sets of 2000, 1500 and 1000 holes each with a diameter of about 100 μm was made for the experiment. The design was transferred to the resist layer using Intelligent micropatterning SF100 XPRESS on a standard non-contact photo-lithography mask-blank. A standard chrome etchant was used to transfer the pattern to the chromium layer. Only a small area ($\sim 64 \text{ mm}^2$) consisting of about 2000 holes of the mask was unblocked while the rest of the areas were blocked by a black tape. An ultra-high-speed camera (Phantom v2512, monochrome, $800 \times 1280, \Delta = 28 \mu\text{m}$) was mounted at a distance of about 15 cm from the occlusion.

For this tutorial study, a spark was generated by capacitor discharge using a simple circuit, as shown in Figure 5a. The circuit consisted of two 10 W, 10 Ω resistors connected in series with a capacitor 100 μF , 400 V [25]. The capacitor was charged to about 207 V and discharged by touching the wires that were connected parallel to the terminals of the capacitor resulting in a sudden discharge causing a spark. This spark event was located approximately 5 cm from the occlusion. The photograph of the experimental set up is shown in Figure 5b. The camera was configured to record the 2 s preceding that start of the fast transient event and triggered manually and saved as a cine file. The Phantom Camera Control software was used to export the cine file into a 12-bit TIFF file for processing in MATLAB. In order to have reliable comparison between invasive and non-invasive approaches, a PSF was recorded using a pinhole with a size of 20 μm at the location of

the event. The image of the recorded green PSF ($\lambda = 530 \text{ nm}$, $\Delta\lambda = 33 \text{ nm}$) and the object intensity distribution of the spark event with a time lapse of $40 \mu\text{s}$ between successive frames are shown in Figure 6a–g.

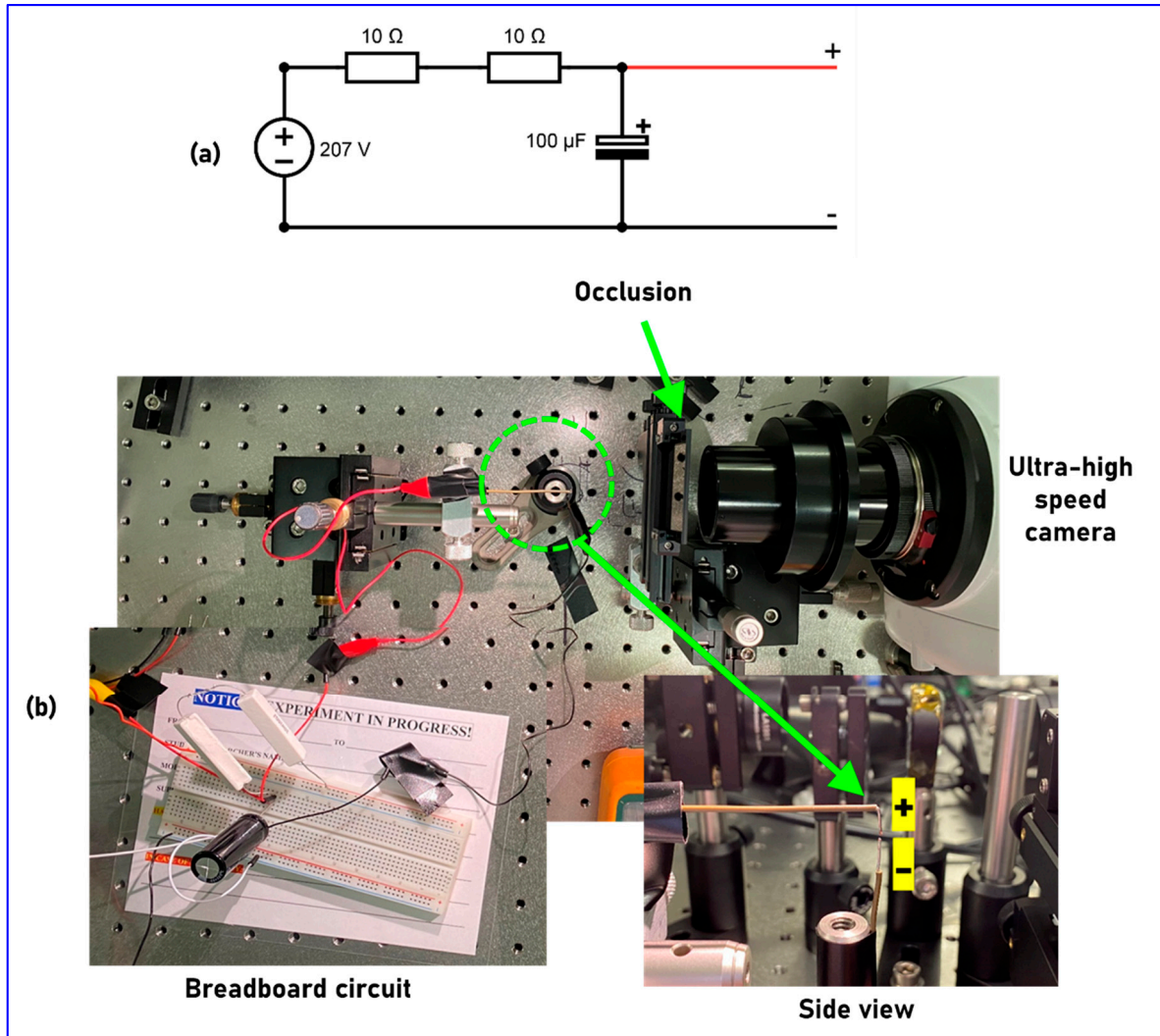


Figure 5. (a) Circuit diagram for generating a spark. (b) Photograph of the experimental set up. A spark event was generated using (a) at a distance of 5 cm from the occlusion and an ultra-high-speed camera was mounted at a distance of 15 cm from the occlusion.

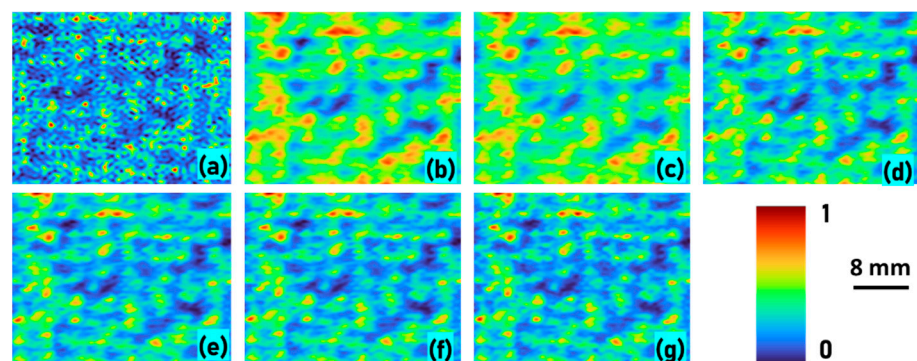


Figure 6. Experimentally recorded green PSF (a), object intensity distributions at $t = 0 \mu\text{s}$ (b), $40 \mu\text{s}$ (c), $80 \mu\text{s}$ (d), $120 \mu\text{s}$ (e), $160 \mu\text{s}$ (f) and $200 \mu\text{s}$ (g).

The reconstructed intensity distributions from invasive and non-invasive approaches are shown in Figure 7. It is seen that the reconstructed intensity distributions from NLR ($\alpha = 0$, $\beta = 0.7$) matched with that of RFA, LRA (50 iterations) and MLA (50 iterations) and the non-invasive method yielded the reconstructions with additional information. The reconstructed intensity distributions for invasive methods enhance the information corresponding to the green wavelength and the corresponding depth which may not happen with the non-invasive approach leading to additional information. The results for non-invasive approach matched with that of the invasive methods for a set of values of the parameters in the phase retrieval algorithm such as spatial frequency range of low-pass filter, computational space and initial guess matrix. However, it was found that the pattern of the initial guess matrix was not crucial if the computational space and filter were optimized. The results obtained did not vary much even when the initial guess matrix consisted of only constant values such as 0 or 1. Furthermore, the number of iterations needed was only about 20 and only mild variations were seen after that indicating a faster convergence which is different from the earlier studies which required hundreds or thousands of iterations [6].

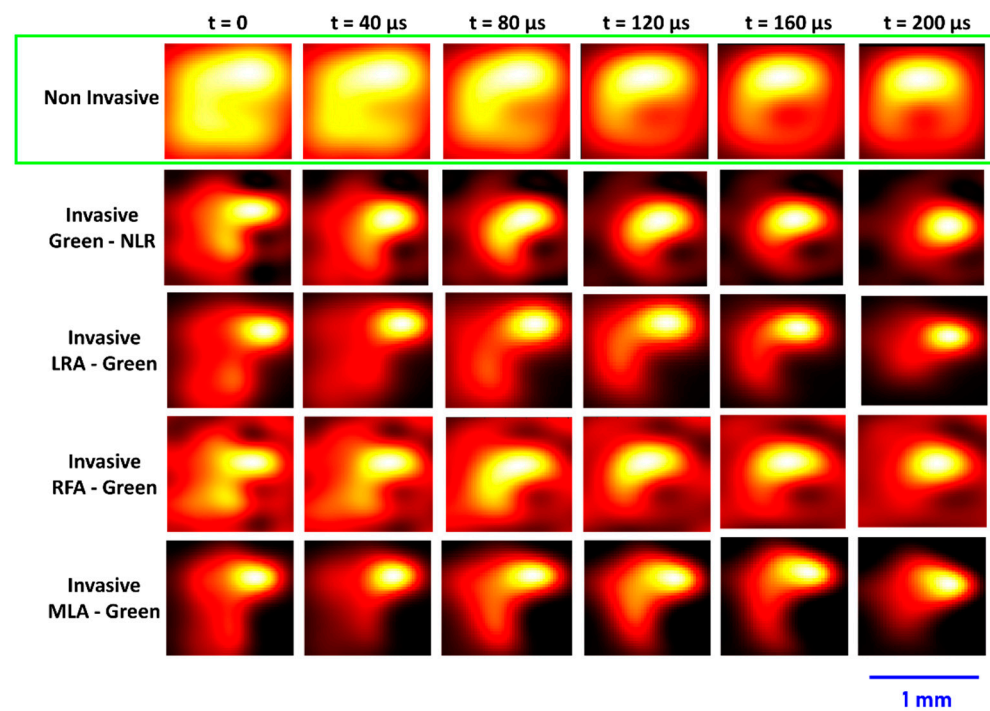


Figure 7. Reconstructed intensity distributions for the spark event separated by $t = 40 \mu\text{s}$ non-invasive and invasive methods NLR, LRA, RFA and MLA for green PSF.

6. Summary and Conclusions

In the recent years, there have been a shift in interest from developing invasive imaging methods towards non-invasive ones. Bypassing the need to record or generate PSFs means that in environments where the target area cannot be accessed, imaging through a scattering or occluding window can still be achieved. Even in situations where conventional imaging is used, the optical window can degrade over time, leading to increased scattering or occlusion and creating an environment highly suitable for this method. This tutorial summarises the invasive and non-invasive methods of image reconstruction and goes through the mathematical operations required to accomplish both. A simple simulation is shown to demonstrate the effects of the occluding medium on the resultant reconstruction, which shows a better result when the occluder is not periodic. Finally, a model system consisting of an electrical spark is used to compare the invasive and non-invasive methods and to show the effects of different filters in the invasive approach. We believe that this

tutorial along with commented code provides good starting point and background for users that want to begin implementing these methods by facilitating quick learning of the fundamentals of invasive and non-invasive approaches for freshman in this area of research. This non-invasive imaging is directly amenable to artificial intelligence analysis of images. The recently developed edge and contrast enhancement studies can be directly applied to the methods discussed here [26].

Supplementary Materials: The following are available online at <https://doi.org/10.5281/zenodo.4882872>, Supplementary files Supplementary_Code_1 and Supplementary_Code_2.

Author Contributions: Conceptualization, V.A.; methodology, V.A.; software, V.A.; validation, V.A. and S.H.N.; Experiments, S.H.N., V.A. and T.K.; resources, S.J.; data curation, V.A. and S.H.N.; writing—original draft preparation, V.A.; writing—review and editing, S.H.N. and S.J.; visualization, S.J.; supervision, S.J.; project administration, S.J.; funding acquisition, S.H.N. and S.J. All authors have read and agreed to the published version of the manuscript.

Funding: Australian Research Council (LP190100505).

Institutional Review Board Statement: Not Applicable.

Informed Consent Statement: Not Applicable.

Data Availability Statement: All data generated or analyzed during this study are included in this published article.

Acknowledgments: The Nano Lab fabrication facility at Swinburne University of Technology is acknowledged.

Conflicts of Interest: The authors declare no conflict of interest.

References

1. Fade, J.; Panigrahi, S.; Carré, A.; Frein, L.; Hamel, C.; Bretenaker, F.; Ramachandran, H.; Alouini, M. Long-range polarimetric imaging through fog. *Appl. Opt.* **2014**, *53*, 3854–3865. [CrossRef] [PubMed]
2. Jaruwatanadilok, S.; Ishimaru, A.; Kuga, Y. Optical imaging through clouds and fog. *IEEE Trans. Geosci. Remote Sens.* **2003**, *41*, 1834–1843. [CrossRef]
3. Paciaroni, M.; Linne, M. Single-shot, two-dimensional ballistic imaging through scattering media. *Appl. Opt.* **2004**, *43*, 5100–5109. [CrossRef]
4. Mukherjee, S.; Vijayakumar, A.; Kumar, M.; Rosen, J. 3D imaging through scatterers with interferenceless optical system. *Sci. Rep.* **2018**, *8*, 1134. [CrossRef] [PubMed]
5. Xu, X.; Xie, X.; Thendiyammal, A.; Zhuang, H.; Xie, J.; Liu, Y.; Zhou, J.; Mosk, A.P. Imaging of objects through a thin scattering layer using a spectrally and spatially separated reference. *Opt. Express* **2018**, *26*, 15073–15083. [CrossRef]
6. Katz, O.; Small, E.; Guan, Y.; Silberberg, Y. Noninvasive nonlinear focusing and imaging through strongly scattering turbid layers. *Optica* **2014**, *1*, 170–174. [CrossRef]
7. Anand, V.; Ng, S.H.; Maksimovic, J.; Linklater, D.; Katkus, T.; Ivanova, E.P.; Juodkazis, S. Single shot multispectral multidimensional imaging using chaotic waves. *Sci. Rep.* **2020**, *10*, 1–13. [CrossRef]
8. Vijayakumar, A.; Rosen, J. Spectrum and space resolved 4D imaging by coded aperture correlation holography (COACH) with diffractive objective lens. *Opt. Lett.* **2017**, *42*, 947–950. [CrossRef]
9. Horisaki, R.; Okamoto, Y.; Tanida, J. Single-shot noninvasive three-dimensional imaging through scattering media. *Opt. Lett.* **2019**, *44*, 4032–4035. [CrossRef]
10. Takasaki, K.T.; Fleischer, J.W. Phase-space measurement for depth-resolved memory-effect imaging. *Opt. Express* **2014**, *22*, 31426–31433. [CrossRef]
11. Singh, A.K.; Naik, D.N.; Pedrini, G.; Takeda, M.; Osten, W. Exploiting scattering media for exploring 3D objects. *Light Sci. Appl.* **2017**, *6*, e16219. [CrossRef]
12. Vijayakumar, A.; Kashter, Y.; Kelner, R.; Rosen, J. Coded aperture correlation holography—A new type of incoherent digital holograms. *Opt. Express* **2016**, *24*, 12430–12441. [CrossRef]
13. Horner, J.L.; Gianino, P.D. Phase-only matched filtering. *Appl. Opt.* **1984**, *23*, 812–816. [CrossRef]
14. Rai, M.R.; Vijayakumar, A.; Rosen, J. Non-linear adaptive three-dimensional imaging with interferenceless coded aperture correlation holography (I-COACH). *Opt. Express* **2018**, *26*, 18143–18154. [CrossRef]
15. Hardie, R.C.; Barnard, K.J.; Ordonez, R. Fast super-resolution with affine motion using an adaptive Wiener filter and its application to airborne imaging. *Opt. Express* **2011**, *19*, 26208–26231. [CrossRef]
16. Richardson, W.H. Bayesian-based iterative method of image restoration. *J. Opt. Soc. Am.* **1972**, *62*, 55–59. [CrossRef]
17. Lucy, L.B. An iterative technique for the rectification of observed distributions. *Astron. J.* **1974**, *79*, 745–754. [CrossRef]

18. Biggs, D.S.C.; Andrews, M. Acceleration of iterative image restoration algorithms. *Appl. Opt.* **1997**, *36*, 1766–1775. [[CrossRef](#)] [[PubMed](#)]
19. Gonzalez, R.C.; Woods, R.E. *Digital Image Processing*; Addison-Wesley Publishing Company, Inc.: Boston, MA, USA, 1992.
20. Anand, V.; Katkus, T.; Lundgaard, S.; Linklater, D.P.; Ivanova, E.P.; Ng, S.H.; Juodkazis, S. Fresnel incoherent correlation holography with single camera shot. *Opto-Electron. Adv.* **2020**, *3*, 200004.
21. Bertolotti, J.; van Putten, E.G.; Blum, C.; Lagendijk, A.; Vos, W.L.; Mosk, A.P. Non-invasive imaging through opaque scattering layers. *Nature* **2012**, *491*, 232–234. [[CrossRef](#)]
22. Mukherjee, S.; Vijayakumar, A.; Rosen, J. Spatial light modulator aided noninvasive imaging through scattering layers. *Sci. Rep.* **2019**, *9*, 17670. [[CrossRef](#)] [[PubMed](#)]
23. Goodman, J.W. *Introduction to Fourier Optics*; Roberts and Company Publishers: Greenwood Village, CO, USA, 2005.
24. Fienup, J.R. Phase retrieval algorithms: A comparison. *Appl. Opt.* **1982**, *21*, 2758–2769. [[CrossRef](#)] [[PubMed](#)]
25. Vijayakumar, A.; Ng, S.H.; Katkus, T.; Juodkazis, S. Spatio-spectral-temporal imaging of fast transient phenomena using a random array of pinholes. *Adv. Photo Res.* **2021**, *2*, 2000032.
26. Anand, V.; Rosen, J.; Ng, S.H.; Katkus, T.; Linklater, D.P.; Ivanova, E.P.; Juodkazis, S. Edge and Contrast Enhancement Using Spatially Incoherent Correlation Holography Techniques. *Photonics* **2021**, *8*, 224. [[CrossRef](#)]